ROYAL SOCIETY
OF CHEMISTRY

PAPER
Halan Prakash *et al.*
Nano-TiO$_2$ immobilized polyvinylidene fluoride based
spongy-spheres for ciprofloxacin photocatalytic degradation:
antibacterial activity removal, mechanisms, UVA LED
irradiation and easy recovery

PAPER

Check for updates

Nano-TiO$_2$ immobilized polyvinylidene fluoride based spongy-spheres for ciprofloxacin photocatalytic degradation: antibacterial activity removal, mechanisms, UVA LED irradiation and easy recovery†

Laxman G. Raikar, [iD] [a] Atul Patel, [iD] [a] Jemi Gandhi,[a] K. V. K. Gupta[b] and Halan Prakash [iD] *[a]

TiO$_2$ is promising for the photocatalytic treatment of water contaminated with organic micropollutants. However, it is hard to recover TiO$_2$ slurry from water. Energy-intensive separation methods are required to recover TiO$_2$, which is a setback in the effective use of TiO$_2$ in water treatment. Herein, we present nano-TiO$_2$ immobilized with polyvinylidene fluoride spongy beads (TP) *via* simple phase inversion of the mixture of TiO$_2$ (1%), PVDF (13%) and PVP (0.7%) for the degradation of ciprofloxacin (CIP), a micropollutant in water, under UVA LED irradiation with easy TP recovery. The stable immobilization of TiO$_2$ with PVDF beads is attributed to interactions between Ti and F atoms. The pseudo first-order rate constant value (k_{obs} = 0.0761 min^{-1}) was determined for the degradation of CIP by TP. Radical scavenging, chronoamperometry, and ESR analysis revealed the presence of O$_2^{-•}$, h$^+$, HO$^•$ and ^{1}O$_2$ reactive species. LC-HRMS analysis detected ten degradation byproducts with possible degradation pathways. Importantly, the antibacterial activity of CIP against *Bacillus subtilis* and *Escherichia coli* was totally removed after 60 min treatment. TP beads were easily recovered using a simple strainer. TP was recovered and reused 30 times, and the absence of significant TiO$_2$ leaching into water demonstrated its stable immobilization. TP photocatalysis under UVA LED irradiation proves an energy-efficient treatment method with an electrical energy per order of 24.20 kW h m^{-3}. Overall, the study highlights a concrete way to effectively use the TiO$_2$ photocatalyst for water treatment *via* immobilization using a simple phase inversion method.

Environmental significance

TiO$_2$ is an excellent photocatalyst for water treatment. However, it is difficult to separate TiO$_2$ slurry from water, which hinders TiO$_2$ recovery and its effective use. Herein, we demonstrate that TiO$_2$ immobilized with PVDF (TP) beads suspended in water exhibits excellent photocatalytic degradation of ciprofloxacin (CIP), a micropollutant of major concern, promoted under energy-efficient UVA LED irradiation. Further, the antibacterial activity of CIP was removed after treatment, highlighting the potential of TP photocatalytic treatment to prevent the risk of antimicrobial-resistant bacteria spreading into the environment due to antibiotics in water. Importantly, easily suspended TP beads were recovered by a simple strainer and reused several times. The study reveals the effective use of nano-TiO$_2$ for water treatment by its immobilization with PVDF beads.

1. Introduction

Organic micropollutants in water are a major concern as they have potential to cause adverse effects on the environment and health.[1] Importantly, the release of

antibiotic micropollutants into water has the risk of leading to the emergence of antibiotic-resistant bacteria (ARB).[2] Ciprofloxacin (CIP) is one of the largely consumed antibiotics across the world.[3] It is mainly used in the treatment of respiratory and urinary tract infections; its incomplete metabolism in the body leads to its large discharge into wastewater and its spread into the environment.[3] CIP belongs to the antibiotic class fluoroquinolones.[3] It has been reported that quinolones are highly non-biodegradable and lead to accumulation in water, thus posing a risk of the spread of ARB.[3]

[a] *Energy and Environmental Chemistry Laboratory, Department of Chemistry, Birla Institute of Technology and Science, Pilani, K. K. Birla Goa Campus, NH17B, Zuarinagar, Goa, 403726, India. E-mail: halanprakash@goa.bits-pilani.ac.in*
[b] *Kwality Photonics Pvt. Ltd., Kushaiguda, Hyderabad, 500062, India*
† Electronic supplementary information (ESI) available. See DOI: https://doi.org/10.1039/d4en00302k

This journal is © The Royal Society of Chemistry 2024

Environ. Sci.: Nano, 2024, 11, 3729–3743 | 3729

Advanced oxidation processes (AOPs) have acquired utmost attention owing to their ability of removing organic micropollutants from water through the *in situ* generation of reactive oxygen species, primarily hydroxyl radicals (HO$^{\bullet}$).[4] Photocatalysis-based AOPs have been widely explored for water treatment.[5] TiO$_2$ is one of the majorly explored photocatalysts for water treatment owing to its abundance in the earth's crust, chemical stability, excellent activity, suitable energy band positions, nontoxicity, and low cost.[6] Importantly, TiO$_2$-based AOPs are known to oxidize organic micropollutants due to the highly reactive HO$^{\bullet}$ together with other oxidative species such as super oxide radicals (O$_2{}^{\bullet-}$) and photogenerated holes (h$^+$).[7] TiO$_2$-based AOPs have the ability to be promoted by energy-efficient LED sources.[8] Moreover, surface adsorption leading to interaction between contaminants and TiO$_2$ for degradation has been reported.[5] Nevertheless, it is important to note that TiO$_2$ suspension is highly stable.[9] Slurry-type photocatalytic systems suffer from the drawback of poor light penetration throughout the photocatalytic chamber due to scattering and inner filter effects and require careful optimization of the initial catalyst dose.[9] Also, the requirement for energy intensive and costly filtration setups for the recovery of the TiO$_2$ catalyst post catalysis is a constraint.[9] Therefore, the recovery of the TiO$_2$ photocatalyst remains a challenge and needs to be well explored.

On the other hand, polyvinylidene fluoride (PVDF) is a well explored membrane material used for water treatment.[10] PVDF is largely used in membrane water treatment systems due to its great chemical stability and higher mechanical strength.[11,12] Additionally, PVDF, being inert to ultraviolet radiations, has the advantage to be used along with TiO$_2$ for UVA-based photocatalytic water treatment systems.[12] Earlier, TiO$_2$-PVDF systems were mainly studied as membrane films for photocatalysis that still require the energy-consuming pressurized filtration step.[13,14] Herein, we propose TiO$_2$ immobilization with PVDF beads by the simple phase inversion technique. The proposed TiO$_2$-immobilized polymeric beads may have dynamic movement throughout the photocatalytic chamber, effective light exposure, and easy recovery without any energy-intensive processes. Earlier, TiO$_2$ immobilized with beads made up of alginate,[15] modified-alginate,[16,17] cellulose aerogels,[18] SiO$_2$[19]-based bead, *via* cross-linking[15–18] and adsorption techniques[19] have been reported. Further, the photocatalysis with these reported TiO$_2$ immobilized beads were studied using conventional light sources like mercury and xenon lamps that consume large electrical energy. Moreover, their stability and evaluation of recoverability for the effective use of photocatalysts need to be well studied.

Based on the above facts, for the first time, we aimed to synthesize TiO$_2$-PVDF polymeric beads (TP) by the simple phase inversion technique and investigate its ability to degrade ciprofloxacin (CIP) antibiotic micropollutant under UVA LED irradiation and photocatalyst recovery. The beads were characterized by different techniques, such as FESEM-EDX, XRD, IR, UV-DRS, XPS, and BET. Different parameters such as the effect of TiO$_2$ loading in TP polymeric beads,

effect of the hydrophilicity inducing agent PVP, and the pH effect on the photocatalytic degradation efficiency were presented. The recovery of TP beads by a simple strainer was discussed. The recyclability of the TP beads along with ICP-AES analysis was performed to determine the stability of the proposed beads. Radical scavenging, ESR and electrochemical results were obtained, and a degradation mechanism was proposed. The results of LC-HRMS analysis and antibacterial assay before and after treatment were presented. Further, the electrical energy per order (EEo) value was determined.

2. Materials and methods

2.1. Reagents

Ciprofloxacin hydrochloride hydrate (CIP) and titanium dioxide nanopowder (TiO$_2$) were obtained from SRL Pvt. Ltd., India. Polyvinylidene fluoride (PVDF) was obtained from Kynar HSV 900, Arkema, polyvinylpyrrolidone (K85-95) (PVP) was obtained from Acros Organics (Fisher scientific), sodium chloride, sodium sulfate, sodium hydroxide, sulfuric acid, iron(III) nitrate nonahydrate, sodium hydrogen carbonate, sodium hydrogen phosphate, and humic acid were obtained from Qualigens, Thermo Scientific. *tert*-Butanol (TBA) (AR, 99%), methanol (MeOH) (HPLC Gradient Grade, 99.9%), and acetonitrile (ACN) (HPLC Gradient Grade, 99.9%) were purchased from Finar, India. Standard pH solutions (pH = 4.01, 7.00, 10.01) obtained from Thermo Scientific were used for calibration of the pH meter. Dimethyl-1-pyrroline-*N*-oxide (DMPO), 1-methyl-2-pyrrolidone (NMP), and 2,2,6,6,-tetramethylpiperidine (TEMP) were purchased from Tokyo Chemical Industry Co., Ltd. (TCI), India. 2,2,6,6-tetramethylpiperidine-1-oxyl (TEMPO) was purchased from Sigma Aldrich. The solutions were prepared in deionized water.

2.2. Synthesis of polymer beads

0.9 g of PVDF (13% w/v) was dissolved in 7 mL NMP solution along with 0.05 g of PVP (0.7% w/v) and stirred for 8 hours at 60 °C, as reported in the earlier literature, to achieve a homogenous slurry of PVDF.[10] The polymer slurry was degassed for 12 hours in a vacuum desiccator. The degassed solution was taken in a syringe and dropped at 10 cm height into water to achieve spherical polymeric beads by phase inversion. These beads were designated as PP beads. Beads synthesized without PVP were labeled as PVDF beads. The average diameter of the beads was measured to be ~2 mm.

2.3. Synthesis of polymer beads with TiO$_2$

To obtain polymeric beads with TiO$_2$, an appropriate amount of TiO$_2$ was taken in a 10 mL NMP and sonicated for 30 min to achieve a homogeneous suspension.[10] Then, this sonicated solution was added to the PP polymer slurry (as mentioned in the above section) with constant stirring at 60 °C. The whole slurry was further stirred for 4 hours at 60 °C. The mixture was subjected to degassing in a vacuum desiccator for 12 hours. The degassed solution was dropped into water

by a syringe to form TP beads *via* phase inversion. TP beads with different loading amounts of TiO$_2$ (1%, 5%, 10% and 15%) were synthesized. TP beads with 1% TiO$_2$ loading with different amounts of PVP (0.35, 0.7, 1.4, 2.1 and 2.5) additive were also synthesized.

2.4. Characterization

Scanning electron microscopy (SEM) and energy dispersive X-ray (EDX) analysis were carried out using a Quanta FEG 250 (FE-SEM) equipped with an area mapping spectrometer (EDX). A LEICA EM ACE 200 sputter coater was used for sputtering the sample for surface analysis and elemental composition. Transmission electron microscopy (TEM) images were acquired using a JEOL model JEM-F200/F2 Multi-purpose Electron Microscope (200 kV). Samples for TEM analysis were prepared by drop casting the dispersion of sonicated TiO$_2$ nanopowder ethanolic solution over carbon-coated copper grids and drying under ambient atmosphere. The surface area, pore volume and size distribution were analyzed by the Brunauer–Emmett–Teller (BET) method using an Anton Paar Quantachrome NOVA 1000e through the nitrogen adsorption–desorption method. The structural properties of the PVDF beads and TiO$_2$ were determined by powder X-ray diffraction (XRD) using a Bruker D8 Advance instrument. The analysis was acquired from 2θ = 10–90 at 5° min^{-1} scanning speed with Cu Kα radiation (λ = 1.5405 Å). The IR spectra were recorded using a Shimadzu FT-IR spectrometer. X-ray photoelectron spectroscopy (XPS) analysis was carried out to identify the surface composition, chemical state of the elements and the interaction between the catalyst and polymer matrix using a K-alpha Thermo Fisher Scientific instrument. A Shimadzu UV-2450 spectrometer was used for the measurement of the UV-visible diffuse reflectance spectra (UV-DRS) for the solid samples with BaSO$_4$ reference in the 200 to 800 nm range. The band gap of TiO$_2$ in TP beads was calculated as per the Tauc eqn (1).[20]

$$\alpha h v = A(h v - E_{\mathrm{g}})^n \tag{1}$$

where α is the absorption coefficient, hv is the energy of incident photon, A is the proportionality constant, $n = \frac{1}{2}$ for direct allowed bandgap, and E_{g} is the band gap.[20] The band gap was predicted from the extrapolation of the linear portion in the graph of $(\alpha h v)^2$ *vs.* hv.[20]

A JEOL Electron spin resonance (ESR) spectrometer was used to record the ESR spectra. Spin trapping agents such as DMPO, TEMPO and TEMP were used for the analysis. The microwave frequency = 9.440 GHz, microwave power = 0.995 mW, and magnetic centre field = 336 mT condition were used. Samples were withdrawn at appropriate time intervals and analysed.

Inductively Coupled Plasma-Atomic Emission Spectrometry (ICP-AES) analysis was carried out using a SPECTRO ARCOS simultaneous ICP spectrometer. The instrument had a minimum detection limit of 10 ppb (μg

L^{-1}) for titanium (Ti). The TP beads were separated from water after photocatalysis using a simple strainer, and the water sample was analysed by ICP-AES.

Electrochemical analysis was performed using a BioLogic SP-150e electrochemical workstation. A three-electrode electrochemical cell was used for chronoamperometric measurements and electrochemical impedance spectroscopy (EIS) for constructing the Mott–Schottky and Nyquist plots. The Mott–Schottky plots were obtained by EIS measurements from −1.0 V to 0 V against Ag/AgCl reference electrode with frequency in the range from 100 kHz to 10 Hz. For the photocatalyst-working electrode, the TiO$_2$ slurry was prepared in water–ethanol mixture using alcoholic Nafion as a binder and coated over fluorine-doped tin oxide (FTO) glass slides over an area of 1 cm^2. In case of TP, the coating slurry was prepared using NMP as the solvent. The reference electrode was Ag/AgCl (saturated KCl) electrode and graphite was used as the counter electrode. 15 mL of 0.1 M Na$_2$SO$_4$ electrolyte solution and 367 nm LED light source was used for all the photoelectrochemical experiment.

The porosity (ε) of the prepared beads was measured by gravimetric analysis (eqn (2)).[21] The water holding capacity can be related to the free volume available over the bead surface and affinity towards water molecules.

$$\varepsilon(\%) = \frac{\frac{W_{\mathrm{wet}} - W_{\mathrm{dry}}}{\rho_{\mathrm{water}}}}{\frac{W_{\mathrm{wet}} - W_{\mathrm{dry}}}{\rho_{\mathrm{water}}} + \frac{W_{\mathrm{dry}}}{\rho_{\mathrm{pvdf}}}} \times 100\% \tag{2}$$

where, W_{wet} and W_{dry} is the weight of wet and dry bead, respectively, and ρ_{water} (0.998 g cm^{-3}) and ρ_{pvdf} (1.785 g cm^{-3}) are the density of water and PVDF, respectively.

2.5. Photocatalysis

All the photocatalysis experiment were performed in deionised water. In a typical reaction, 50 mL of water was spiked with 1 ppm (1 mg L^{-1}) CIP and appropriate number of TP beads were added in the solution. An ultraviolet A light emitting diode (UVA LED) with maximum wavelength (λ_{max}) at 367 nm was used as the light source. A UVA LED light source was placed at a distance of 5 cm over the water surface for uniform irradiation with an average irradiance of 3.5 mW cm^{-2}. A stock solution of 100 ppm (100 mg L^{-1}) of CIP was used for all the analysis. For studying the pH effect, 0.1 N HCl and 0.1 N NaOH were used to adjust the pH. In real water matrix analysis, municipality tap water and simulated ground water were used (SGW). The characteristics of municipality tap water are provided in Table S1.† The SGW was prepared as per an earlier report.[22] The composition of SGW was as follows: Fe (NO$_3$)$_3$·9H$_2$O = 0.24 μM (0.096 mg L^{-1}), NaHCO$_3$ = 1.2 mM (100 mg L^{-1}), Na$_2$SO$_4$ = 0.34 mM (48.29 mg L^{-1}), Na$_2$HPO$_4$ = 0.28 mM (40 mg L^{-1}), NaCl = 0.86 mM (50 mg L^{-1}), humic acid = 10.0 mg L^{-1}.[22]

The degradation of CIP was monitored by high performance liquid chromatography (HPLC); the HPLC method conditions are discussed in Text S1.† 0.5 mL sample aliquot was collected at 10 min intervals and injected in the HPLC instrument. The

This journal is © The Royal Society of Chemistry 2024

Environ. Sci.: Nano, 2024, **11**, 3729–3743 | **3731**

degradation byproducts were screened using a high resolution mass spectrometer (LC-HRMS-ToF). The method conditions are described in Text S2.† 2 mL sample aliquot was withdrawn after 60 min of photocatalysis reaction and used for analysis. A EUTECH pH 700 meter was used to measure the solution pH. For the radical scavenging experiment, benzoquinone (BQ), ethylenediaminetetraacetic acid disodium salt (EDTA), sodium azide (NaN$_3$), and *tert*-butyl alcohol (TBA) were used for the scavenging of the superoxide radical (O$_2$$^-$), photogenerated holes (h$^+$), singlet oxygen (^{1}O$_2$), and hydroxyl radical (HO$^\cdot$), respectively.[23] 10 mM scavengers were spiked in the reaction mixture for the studies.

2.6. Antibacterial assay

The antibacterial activity of CIP was determined by the agar well diffusion method as per Clinical and Laboratory Standards Institute (CLSI)[24] before and after the treatment with different time intervals by TP beads as per the standard protocol.[24] The Gram-positive *Bacillus subtilis* and Gram-negative *Escherichia coli* bacterial strains were used to evaluate the antibacterial activity of CIP. 90 mm sterile petri dishes were used to prepare plates with 22 mL of nutrient agar to yield 4 mm depth media. The standard spread-plate technique employed 100 μL of inoculum suspension on the solid media plates. Round wells (8 mm in diameter) were punched into agar plates using a sterile well-borer. The wells were filled with 75 μL of the samples using a sterile micropipette. These plates were incubated for 24 h at 37 °C and the inhibition zone (mm) around the well was measured. Experiments were repeated three times and the standard error was calculated.[22]

3. Results and discussion

3.1. Characterization of polymer beads

3.1.1. SEM–EDX analysis of polymeric beads. The SEM image of the spherical PP bead reveals the average diameter to be about 2 mm (Fig. 1a). Further, 1000× magnification images reveal that the surface of the bead is porous in nature (Fig. 1b). The cross-section image reveals pores on the surface and channels and large voids spaces inside the bead; overall, the bead has a sponge-like morphology (Fig. 1c). The internal void space is much greater than the surface pore openings (Fig. 1b and d). Earlier, porous PVDF membrane flat sheet with large internal voids, as observed in the present study, was reported.[25] The SEM images of the whole TP bead and its corresponding cross-sectional image (Fig. 1e–h) were very similar to that of the PP bead (Fig. 1a–d). The SEM images for beads with different TiO$_2$ loading reveals no significant change in the morphology of the beads (Fig. S1†). Importantly, the SEM-EDX image results clearly reveal that TiO$_2$ was partially distributed on the surface of the beads as well as in the internal void spaces (Fig. S2†). Moreover, the SEM images reveal that the addition of PVP, a known hydrophilic polymer additive, induced more surface pores, leading to a rougher surface of the TP beads (Fig. S3†).[26,27] Additionally, the distribution of TiO$_2$ nanoparticles on the surface of the TP beads were not affected by PVP loading, as revealed by SEM EDX analysis (Fig. S4†). Further, a magnified SEM image reveals that TiO$_2$ has a grain-like morphology with an average partial size of 25 nm that was agglomerated into large irregular clusters, and similar features of TiO$_2$ were seen in TP beads (Fig. S5a† and 1f and h). Further, the TEM image reveals the grain-like morphology of TiO$_2$ nanoparticles (Fig. S5b†). Thus, all the above results reveal the immobilization of TiO$_2$ with the PVDF sponge beads.

3.1.2. BET analysis and porosity determination. The surface area, total pore volume, and pore diameter of PVDF, PP, TP beads and TiO$_2$ are summarized in Table S2.† The surface area of PVDF and PP beads (with and without the addition of PVP, a hydrophilic additive) was 2.7550 m^2 g^{-1} and 4.1065 m^2 g^{-1}, respectively.[26,27] The TP beads had a higher surface area of 8.6374 m^2 g^{-1} compared to that of PVDF beads (2.7550 m^2 g^{-1}). The higher surface area was attributed to the contribution of the immobilized high-surface TiO$_2$ nanoparticles (77.4609 m^2 g^{-1}) on the surface of
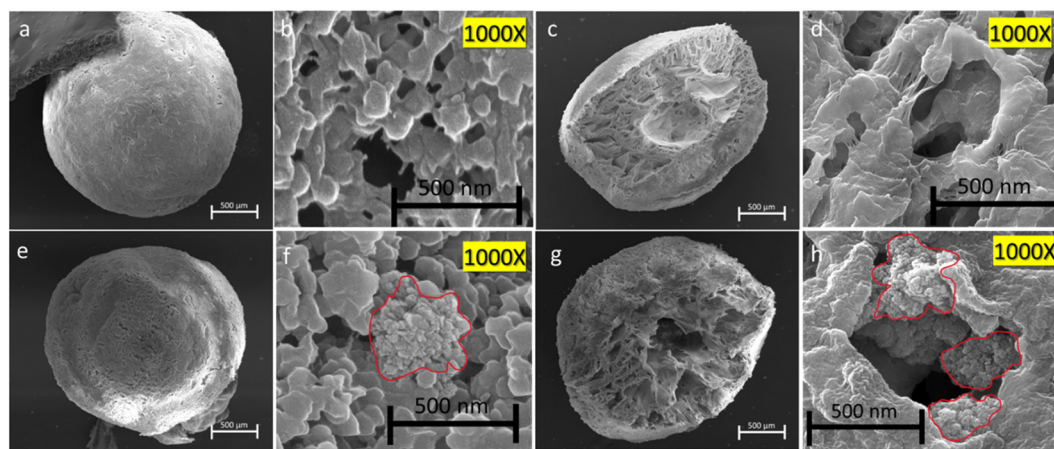

Fig. 1 SEM images of the surface and corresponding cross-section of beads with the respective high magnification images (1000×). PP (a–d) and TP (e–h). TP = 1% TiO$_2$ with PVDF having 0.7% PVP; PP = PVDF having 0.7% PVP.

the beads (Table S2†). Further, the porosity (%) measured by the gravimetric method for the beads was summarized (Table S2†). These results reveal that the porosity was not significantly affected by the immobilization of TiO_2, indicating the TP may exhibit effective mass transfer needed for the photocatalytic degradation of pollutants.

3.1.3. XRD analysis. The X-ray diffraction patterns of the TiO_2, PP, and TP beads were recorded (Fig. 2a). The XRD pattern of TiO_2 displayed peaks at 2θ = 25.4°, 37.0°, 37.9°, 38.6°, 48.1°, 54.0° and 55.2° corresponding to the (101), (103), (004), (200), (105), (211), and (204) planes, respectively, revealing the anatase phase of TiO_2.[28] In case of PP, the peaks at 2θ = 18.5°, 20.4° and 26.4° were attributed to PVDF. The reflection at 18.5° corresponds to the γ (020) plane. The reflection at 20.4° corresponds to (200) and (110) reflections of β overlapped with (021) of the γ phase.[29] The reflection at 26.4° represents the (021) plane of the α phase of PVDF. The XRD pattern of TP displayed characteristic peaks of TiO_2 and PVDF polymer with no major shift in the 2θ values.[28] The crystallite size of TiO_2 calculated using the Scherrer's equation (Text S3†) was found to be 20.9 nm for TiO_2 and 19.7 nm for TP. Thus, the XRD results reveal that the immobilized TiO_2 in the TP bead had a structure similar to the parent TiO_2 in the anatase form.

3.1.4. IR analysis. The IR spectral results for TiO_2, PP and TP are presented in Fig. 2b. The IR spectrum of TiO_2 shows characteristic strong intense peak at about 420 cm^{-1} to 490 cm^{-1} for the Ti–O stretching frequency.[30] In case of PP, the IR peaks at 488 cm^{-1}, 615 cm^{-1}, 763 cm^{-1}, 877 cm^{-1}, 976 cm^{-1}, and 1401 cm^{-1} resulted from the α phase of the PVDF.[31] The peaks at 841 cm^{-1}, 1072 cm^{-1}, 1277 cm^{-1} and 1430 cm^{-1} correspond to the β phase. The γ phase is represented by the peak at 1179 cm^{-1}.[31] TP shows a broad Ti–O peak in the range from 420 cm^{-1} to 490 cm^{-1}. The peak with maximum intensity at 1673 cm^{-1} represents the pyrrolidone carbonyl stretching frequency of the PVP

molecule.[32] Importantly, the ratio of β (at 841 cm^{-1}) and α (at 763 cm^{-1}) peaks observed in PVDF was found to be enhanced after the immobilisation of TiO_2 in TP, revealing the interaction between TiO_2 and PVDF. Earlier, a similar observation was reported for the TiO_2 immobilized with PVDF membrane in the flat sheet form.[33] Further, the possible interaction between TiO_2 and PVDF was investigated by XPS analysis, as discussed below.

3.1.5. XPS analysis. The XPS spectra of the TiO_2 core level Ti 2p showed two peaks at 459.55 eV and 465.16 eV corresponding to Ti $2p_{3/2}$ and Ti $2p_{1/2}$, respectively (Fig. 3a). In TP, the Ti $2p_{3/2}$ and Ti $2p_{1/2}$ peaks were observed at 458.68 eV and 464.41 eV, respectively. The shifts in the Ti $2p_{3/2}$ and Ti $2p_{1/2}$ peaks of TP compared to TiO_2 indicate the interaction between Ti and the polymer matrix.[34] Further, PP showed a single peak of F 1s at 688.08 eV corresponding to the C–F bond of PVDF (Fig. 3b). Importantly, the C–F peak in case of TP beads was also observed. However, the F 1s peak position was at 687.96 eV (Fig. 3b), corresponding to a shift of 0.12 eV compared to the PP beads. These observations reveal the interaction between Ti and F in TP. Interestingly, a small hump at about 684.22 eV was observed, which is attributed to Ti–F interaction.[34] Similar results were observed in case of PVDF-modified TiO_2 prepared *via* the chemisorption of PVDF on to TiO_2.[34] The O 1s spectra showed peaks at 530.73 eV and 532.45 eV for TiO_2 resulting from Ti–O–Ti and O–H bonding, respectively. The peaks at 531.61 eV and 532.82 eV were attributed to functional groups C–O/C=O and O–H, respectively (Fig. 3c).[35] The O–H was mainly because of the trapped water molecules during the phase inversion of the polymer into beads (Fig. 3c). The Ti-O-Ti peak of TP was shifted by 0.9 eV compared to TiO_2, confirming the strong influence of the highly electronegative F atom on the Ti atom.[34] The C 1s spectra of PP showed peaks at 285.36 eV, 286.52 eV, 287.64 eV and 291.02 eV for the C–C, C–H, C–O and C–F bonds, respectively (Fig. 3d).[35] In the case of TP, the C 1s peaks were identified with no major shift in the signals
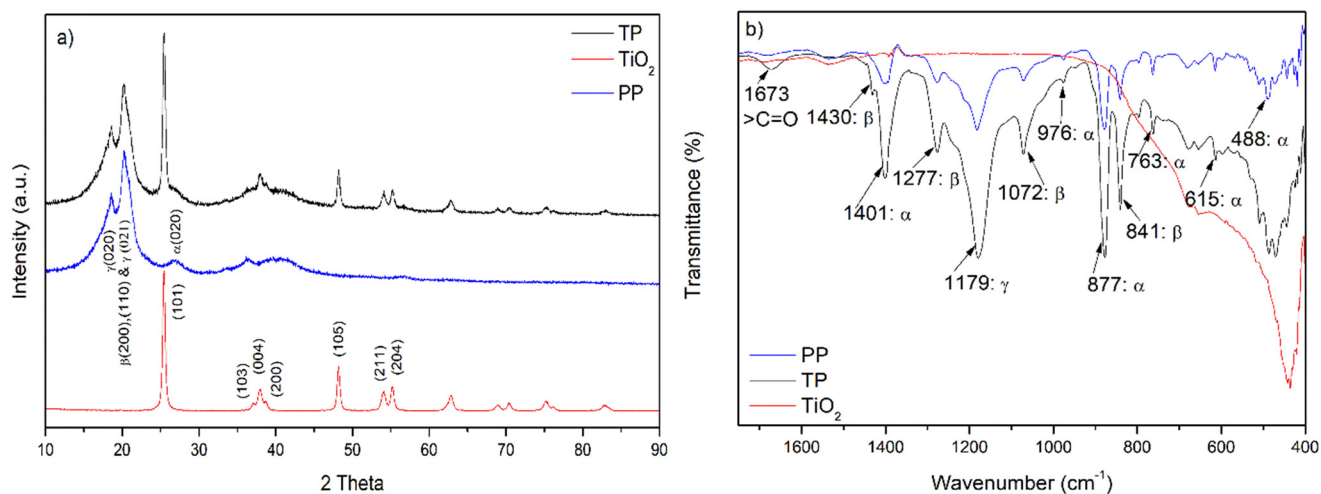

Fig. 2 a) XRD pattern of TiO_2, PP and TP beads. b) IR spectra of TiO_2, PP and TP beads. TP = 1% TiO_2 with PVDF having 0.7% PVP; PP = PVDF having 0.7% PVP.

This journal is © The Royal Society of Chemistry 2024

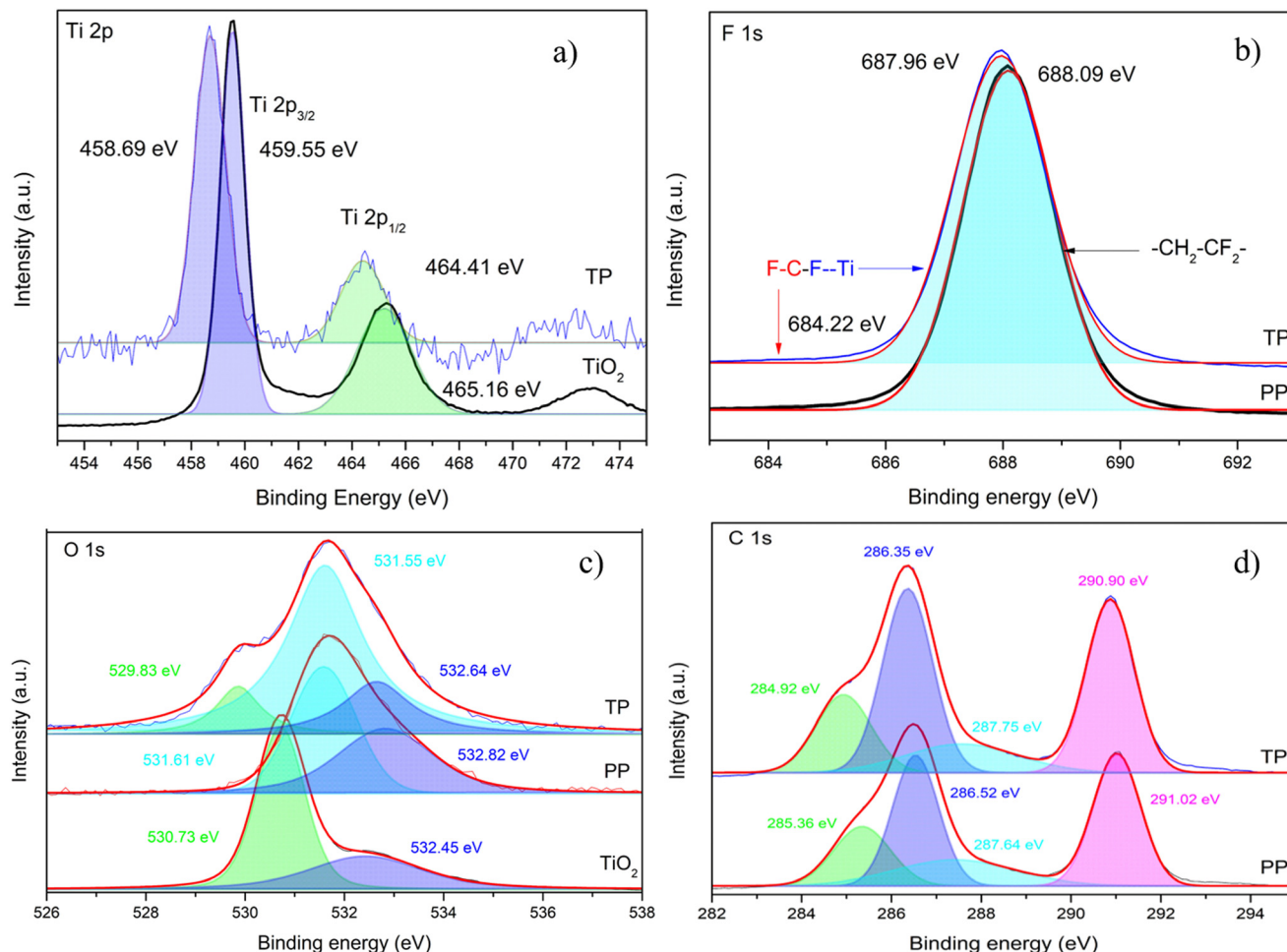*Environ. Sci.: Nano*, 2024, **11**, 3729–3743 | **3733**

Fig. 3 XPS spectra of the core levels: a) Ti 2p, b) F 1s, c) O 1s, d) C 1s for TiO_2, PP and TP. TP = 1% TiO_2 with PVDF having 0.7% PVP; PP = PVDF having 0.7% PVP.
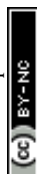
compared to the PVDF beads. The XPS survey spectra for TiO_2, PP and TP are presented in Fig. S6.† Overall, XPS analysis clearly reveals the immobilization of TiO_2 with PVDF and the interaction of Ti and F atoms.

3.1.6. Absorption and electrochemical characterization. The band gap of TiO_2 and TP was determined to be 3.24 eV and 3.20 eV, respectively (Fig. S7(a)†). No major difference in the band gap reveals that immobilized TiO_2 has an electronic distribution similar to free TiO_2. Further, the emission spectra of the UVA LED lamp with an emission maximum at 367 nm (corresponding to 3.37 eV) overlaps with the TP absorption spectrum (bandgap (E_g) = 3.26 eV), revealing that UVA LED with 367 nm wavelength is suitable for the promotion of TP photocatalysis (Fig. S7(b)†).[23] The flat band potentials obtained from the Mott–Schottky plot for the free TiO_2 (−0.702 V vs. Ag/AgCl) and immobilized TiO_2 (0.710 V vs. Ag/AgCl) were found to be almost similar (Fig. S8†).[36] Additionally, the Nyquist plot showed a similar arc radius, implying no major difference in the electron transfer ability of the TiO_2 bound to PVDF beads in comparison to free TiO_2 (Fig. S9†).[35,36]

3.2. Photocatalysis

3.2.1. Photocatalytic degradation of CIP by TP under UVA LED irradiation. The CIP molecule was nearly stable under only UVA light irradiation, even after 60 min of photolysis (Fig. 4a). Further, the adsorptive removal of CIP by PP and TP beads was not effective, less than 45% after 60 min of dark incubation. Importantly, only in the case of CIP molecule irradiated under UVA light in the presence of TP caused almost complete degradation within 60 min.[9,17] The pseudo first-order rate constant (k_{obs}) for the degradation of CIP by TP under UVA irradiation was determined to be 0.0761 min^{-1}.[37]

3.2.2. Effect of catalyst loading. TP with different TiO_2 loading (1%, 5%, 10% and 15%) showed no significant difference in the degradation efficiency (Fig. 4b). As discussed in the earlier sections, the cross-sectional SEM images and the corresponding SEM–EDX analysis of the different TP beads revealed the occupancy of TiO_2 inside the large voids of TP beads as the amount of TiO_2 increased (Fig. S1 and S2†). These facts indicate that the available surface exposed TiO_2 were similar, although the TiO_2 loading was varied, and accounted for no change in the k_{obs} values.

Fig. 4 a) Degradation of CIP by TP under UVA LED irradiation, TP = 1% TiO_2 with PVDF having 0.7% PVP, PP = PVDF having 0.7% PVP (control), b) effect of TiO_2 loading on the degradation of CIP by TP under UVA LED irradiation. Experimental conditions: [CIP] = 1 ppm, number of TP beads = 100, TP = 1%, 5%, 10% and 15% TiO_2, reaction volume = 50 mL.

Similar results were reported in the case of TiO_2-gC_3N_4/PVDF flat sheet membranes[38] and KCN/alginate beads[39] as the catalyst loading was increased.

3.2.3. Effect of PVP. The effect of PVP strength over the photocatalytic efficiency of the TP beads is presented in Fig. S10.† The PVP strength was varied from 0% to 2.8% in the TP bead synthesis. At 0 PVP, lower photocatalytic efficiency was noted, with incomplete degradation (90%) at 60 min. Upon increasing the PVP loading in the range from 0.35% to 1.4%, the degradation efficiency gradually increased. Further, at higher PVP loading of 2.1% and 2.8%, a minor reduction in the photocatalytic activity of the TP beads was observed. These results indicate that the appropriate loading of PVP is important. Earlier, PVP has been used as an additive in the phase inversion of PVDF to induce rough surface and hydrophilicity, which facilitates proper mass transfer and

induces efficient photocatalysis.[40] Upon increasing the PVP content, rough surface and enhanced surface pores were observed (Fig. S3†). Nevertheless, the results emphasize that a higher loading (about 2.1%) may cover the TiO_2 nanoparticles distributed on the surface pores and retard the photocatalytic efficiency.[38]

3.2.4. Effect of the initial concentration of CIP. The influence of the initial concentration of CIP is presented in Fig. 5a. As the concentration of CIP is increased from 1 ppm to 5 ppm, there is a reduction in the photocatalytic efficiency. The pseudo first order rate (k_{obs}) value decreases exponentially from 0.0761 min^{-1} to 0.0282 min^{-1} with the increase in the initial concentration of CIP (1–5 ppm) (Table S3,† Fig. 5b). This is mainly due to the limited availability of the active sites of the photocatalyst in comparison to the higher initial concentration of CIP, adsorption of more CIP over the photocatalyst beads,

Fig. 5 a) Effect of initial concentration of CIP on the degradation by TP under UVA LED irradiation. b) Graph of ln(C/C_0) vs. time for the degradation of CIP. Experimental conditions: number of TP beads = 100, TP = 1% TiO_2, 0.7% PVP with PVDF, and reaction volume = 50 mL.

Fig. 7 a) Radical scavenging experiment for the degradation of CIP by TP beads. Experimental conditions: [CIP] = 1 ppm, [TBA] = [p-BQ] = [EDTA] = [NaN$_3$] = 10 mM, number of beads: 100, and TP = 1% TiO$_2$ with PVDF having 0.7% PVP. b) Photocurrent-time dependence curve. Experimental condition: 10 s ON–OFF cycle, voltage = 0.2 V against Ag/AgCl electrode, electrolyte = 0.1 N Na$_2$SO$_4$, and [CIP] = 1 ppm.

Fig. 8 ESR spectra of (a) DMPO–O$_2$$^{-}$, (b) DMPO–HO$^{•}$, (c) TEMPO–h$^+$, and (d) TEMP–^{1}O$_2$ for the light and dark experiment. [TP] = 100 bead/50 mL, [DMPO] = [TEMPO] = [TEMP] = 30 mM, TP = 1% TiO$_2$, and 0.7% PVP with PVDF.
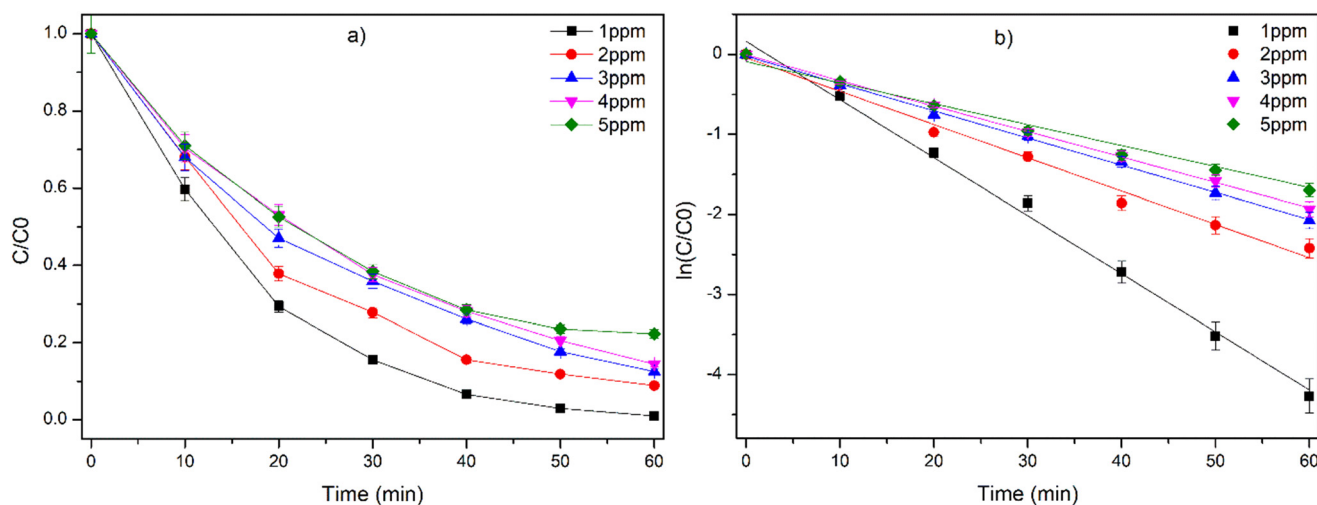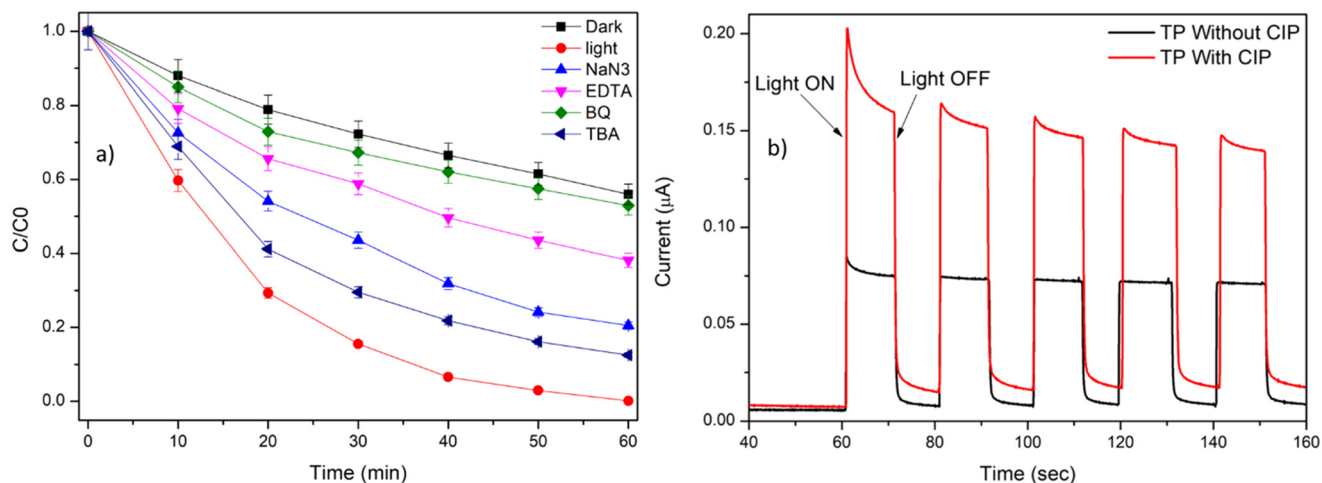
(Fig. 8b).[22,43] TEMPO has a triplet signal in the ESR spectrum due to its paramagnetic nature, and the reduction of the signal intensity during photolysis is attributed to the presence of photogenerated holes (h^+), which oxidizes the TEMPO (Fig. 8c).[43] In t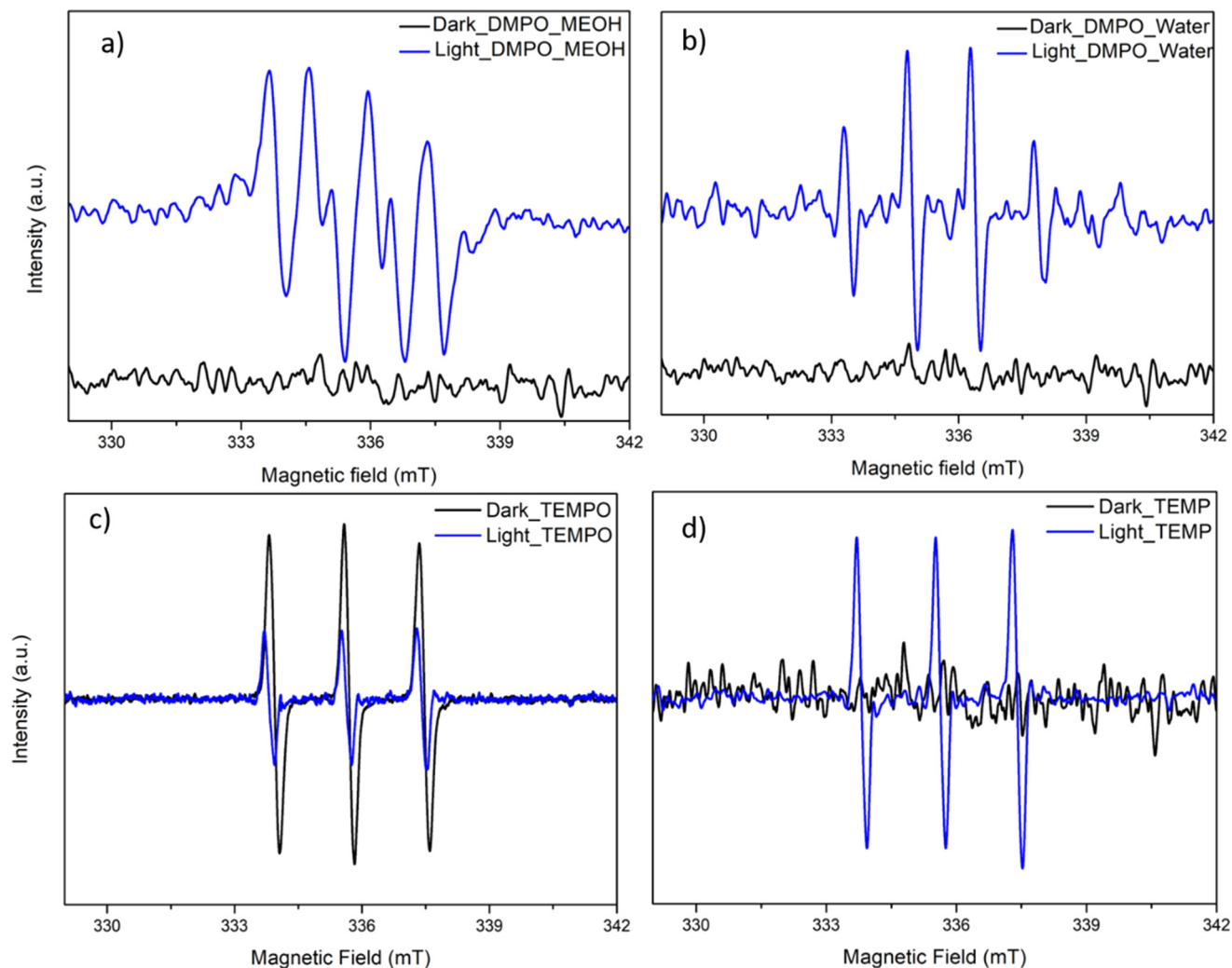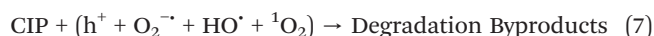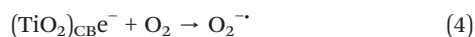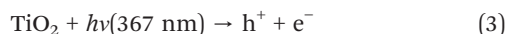he presence of TEMP, singlet oxygen ($^1O_2$) probe, triplet signals of equal intensity were observed, depicting the $^1O_2$ generation by the TP beads under UVA irradiation (Fig. 8d).[43]

Based on all these results, the following photocatalytic mechanism for the generation of reactive species during photolysis and the degradation of CIP is presented below (eqn (3)–(7) and Fig. 9).

$$TiO_2 + h\nu(367\ nm) \rightarrow h^+ + e^- \qquad (3)$$

$$(TiO_2)_{CB}e^- + O_2 \rightarrow O_2^{-\cdot} \qquad (4)$$

$$O_2^{-\cdot} + h^+ \rightarrow {}^1O_2 \qquad (5)$$

$$(TiO_2)_{VB}h^+ + H_2O \rightarrow HO^\cdot \qquad (6)$$

$$CIP + (h^+ + O_2^{-\cdot} + HO^\cdot + {}^1O_2) \rightarrow Degradation\ Byproducts \qquad (7)$$

3.2.7. Degradation in real water matrix. The degradation of CIP in distilled water, simulated ground water (SGW) and real tap water was performed. The degradation efficiency of CIP in SGW and real tap water was determined to be about 74.6% and 94.6%, respectively (Fig. 10). This was attributed to presence of deactivating water constituents such as Cl^-, HCO_3^-, and NOM.[44] The degradation of CIP in the presence of individual water constituents like Cl^-, HCO_3^-, and HA were determined (Fig. S11†). The quenching effect was observed in the order HA > Cl^- ≥ HCO_3^-. Humic acid is known to retard the degradation reaction due to i) the blocking of the active site of the photocatalyst *via* adsorption, ii) a strong absorption in the UV-visible region that leads to the inner filter effect of the UVA irradiations and iii) consuming $HO^\cdot$ and other reactive species generated in the reaction
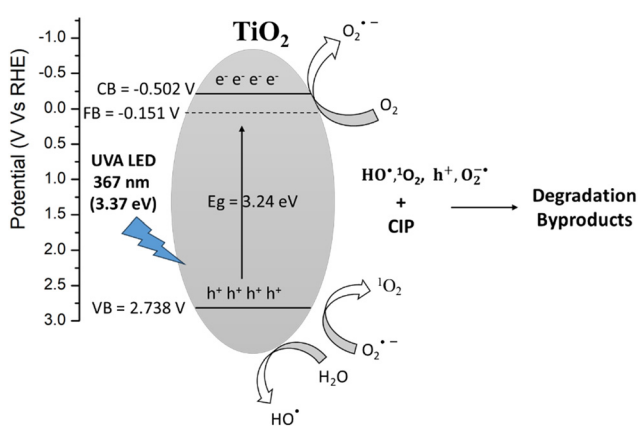

Fig. 10 Degradation of CIP in real water matrix, experimental conditions: [CIP] = 1 ppm, TP = 1% TiO_2, 0.7% PVP with PVDF beads, volume: 50 mL.

system.[44,45] In accordance with the literature, Cl^- and HCO_3^- were reported to react with $HO^\cdot$ and photogenerated hole in TiO_2 photocatalysis to generate secondary radicals such as $Cl_2^{-\cdot}$ and $Cl_3^{-\cdot}$ (eqn (8)–(13)) that are less reactive than $HO^\cdot$, thereby decreasing the degradation efficiency.[46–48]

$$HCO_3^- + HO^\cdot \rightarrow CO_3^{-\cdot} + H_2O \qquad (8)$$

$$HCO_3^- + h^+ \rightarrow CO_3^{-\cdot} + H^+ \qquad (9)$$

$$Cl^- + HO^\cdot \rightarrow ClHO^{-\cdot} \qquad (10)$$

$$ClHO^{-\cdot} + H^+ \rightarrow Cl^\cdot + H_2O \qquad (11)$$

$$Cl^- + h^+ \rightarrow Cl^\cdot + H^+ \qquad (12)$$

$$Cl^\cdot + Cl^- \rightarrow Cl_2^{-\cdot} \qquad (13)$$

The deactivating water constituents in real tap water (HA = below permissible limit, HCO_3^- = 23.6 mg L^{-1}, Cl^- = 13.91 mg L^{-1}) are relatively lower compared to SGW (HA = 10 mg L^{-1}, HCO_3^- = 100 mg L^{-1}, Cl^- = 50 mg L^{-1}). Hence, less negative impact on the degradation efficiency occurs in the case of real tap water compared to SGW (Fig. 10). Earlier similar results have been observed for the photocatalytic activity by slurry TiO_2 nanoparticles.[49]

3.3. Recyclability and stability studies

One major drawback of TiO_2 nanopowder is its recyclability as it forms a stable suspension that does not settle even after a long period of standing. The recovery of the TiO_2 nanopowder requires energy-intensive processes such as centrifugation and filtration, which further involve loss of the catalyst. In the present work, the suspended TP beads were easily recovered

Fig. 9 Photocatalytic mechanism for the degradation of CIP by TP beads under UVA LED irradiation.

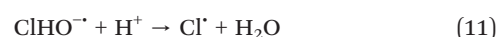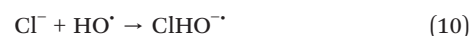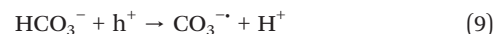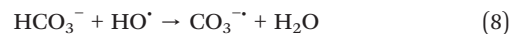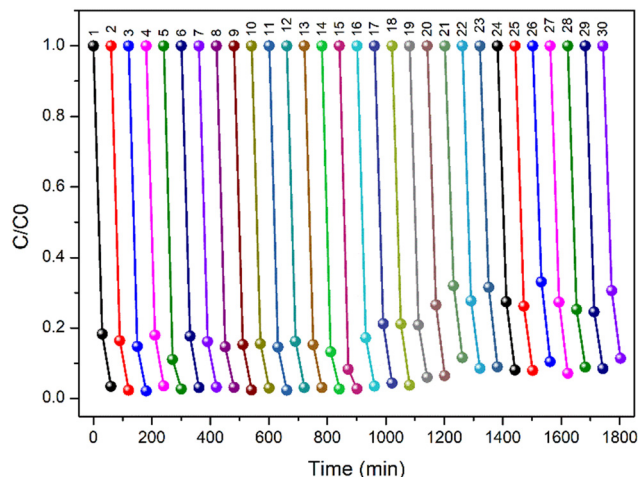**3738** | *Environ. Sci.: Nano*, 2024, **11**, 3729–3743

This journal is © The Royal Society of Chemistry 2024

Fig. 11 Recyclability test of TP bead, experimental conditions: [CIP] = 1 ppm, TP = 1% TiO_2, 0.7% PVP with PVDF beads, and volume: 50 mL.

post photocatalysis using a simple strainer. The recovered beads were investigated for their further use to degrade CIP. The recyclability studies of the TP beads were presented for 30 cycles (Fig. 11). Importantly, there was no reduction in the photocatalytic activity of the beads until 20 cycles. Above 20 cycles, a very small decrease in the photocatalytic activity was observed. At the end of 30 cycles, the efficiency was determined to be 90% (Fig. 11). The slight reduction in efficiency may be attributed to the trace amount of accumulation of organic pollutants over the active site of the photocatalyst.

Further, the stability of immobilized TiO_2 over PVDF beads was monitored by ICP-AES analysis. Importantly, no leaching of TiO_2 was observed for the 30 cycles. The recyclability studies show that TP is highly reusable without the loss of TiO_2 into water. Importantly, the FTIR spectra and SEM images were recorded for used TP beads (Fig. S12 and S13†), respectively. The IR result showed no difference in the functional group of the used TP bead and the SEM images showed the presence of TiO_2 with no change in the surface morphology of the TP beads. All the above results strongly depict the effective use of TiO_2 photocatalyst by the immobilization of TiO_2 catalyst with PVDF beads *via* the simple phase inversion method for water treatment.

3.4. Identification of degradation byproducts of CIP

The LC-HRMS data of degradation byproducts along with the molecular formula, double bound equivalence (DBE) and the ppm error in the formula generated are presented in Table 1. Ten degradation byproducts were identified by LC-HRMS analysis (Scheme 1). The extracted ion chromatograms (EIC) for all the degradation byproducts are presented in Fig. S14–S24.† The plausible degradation pathways are presented in Scheme 1. Piperazine ring oxidation due to the attack by reactive species (O_2^{-}, h^+, $^1O_2$, $HO^{\cdot}$) involving ring opening led to the degradation byproducts (2–8).[50–52] Structures 9 and 10 are the decarboxylated products of 5 and 8, respectively.[52–54] The structure 11 is the defluorinated product of structure 8 (Scheme 1).[51]

3.5. Antibacterial activity removal

The antibacterial activity of CIP before treatment and after treatment (at 20, 40 and 60 min) by TP were determined (Fig. 12). These results reveal that CIP before treatment (0 min) showed the zone of inhibition of 1.8 ± 0.2 cm and 2.5 ± 0.1 cm against the target *B. subtilis* (Fig. 12a) and *E. coli* (Fig. 12b), respectively. A decrease in the zone of inhibition was observed as the treatment time was increased, both in case of *B. subtilis* and *E. coli* organisms. Importantly, there was no zone of inhibition against *B. subtilis* and *E. coli* after 60 min of treatment (Fig. 12). The complete removal of antibacterial activity is important to prevent the risk of antimicrobial resistance bacteria spreading into the environment due to antibiotics in water.

3.6. Electrical efficiency

The electrical energy per order for the TP photocatalytic degradation of CIP under UVA LED irradiation was determined to be 24.20 kW h m⁻³, as discussed in Text S4.† Kokate *et al.*, reported similar EEo values for the degradation of the dye pollutant by the 400 nm LED light source.[55] The lower EEo value depicts the UVA LED as an energy-efficient light source for photocatalytic degradation.[55] To the best of our knowledge, the present study is the first to report a stable immobilization of the TiO_2 photocatalyst with PVDF bead support, which is extensively used as a

Table 1 HR-MS data for the degradation byproducts of CIP

Sr. no	Compound	(RT) (min)	Experimental mass $[(M + H)]^+$	DBE	Mass error (ppm)
1.	Ciprofloxacin $C_{17}H_{18}FN_3O_3$ (**1**)	1.9	332.1408	10	0.82
2.	$C_{17}H_{16}FN_3O_5$ (**2**)	2.0	362.1146	11	0.07
3.	$C_{17}H_{18}FN_3O_4$ (**3**)	2.0	348.0993	11	0.69
4.	$C_{16}H_{16}FN_3O_4$ (**4**)	2.1	334.1199	10	0.40
5.	$C_{16}H_{16}FN_3O_3$ (**5**)	2.4	318.2791	9	−3.96
6.	$C_{15}H_{16}FN_3O_3$ (**6**)	1.8	306.1248	9	0.20
7.	$C_{14}H_{11}FN_2O_4$ (**7**)	2.1	291.0775	10	−0.08
8.	$C_{13}H_{11}FN_2O_3$ (**8**)	2.1	263.0828	9	0.84
9.	$C_{15}H_{16}FN_3O$ (**9**)	1.9	274.0983	9	−0.88
10.	$C_{12}H_{11}FN_2O$ (**10**)	2.3	219.1744	8	−4.36
11.	$C_{13}H_{12}N_2O_3$ (**11**)	2.1	245.0848	9	−4.94
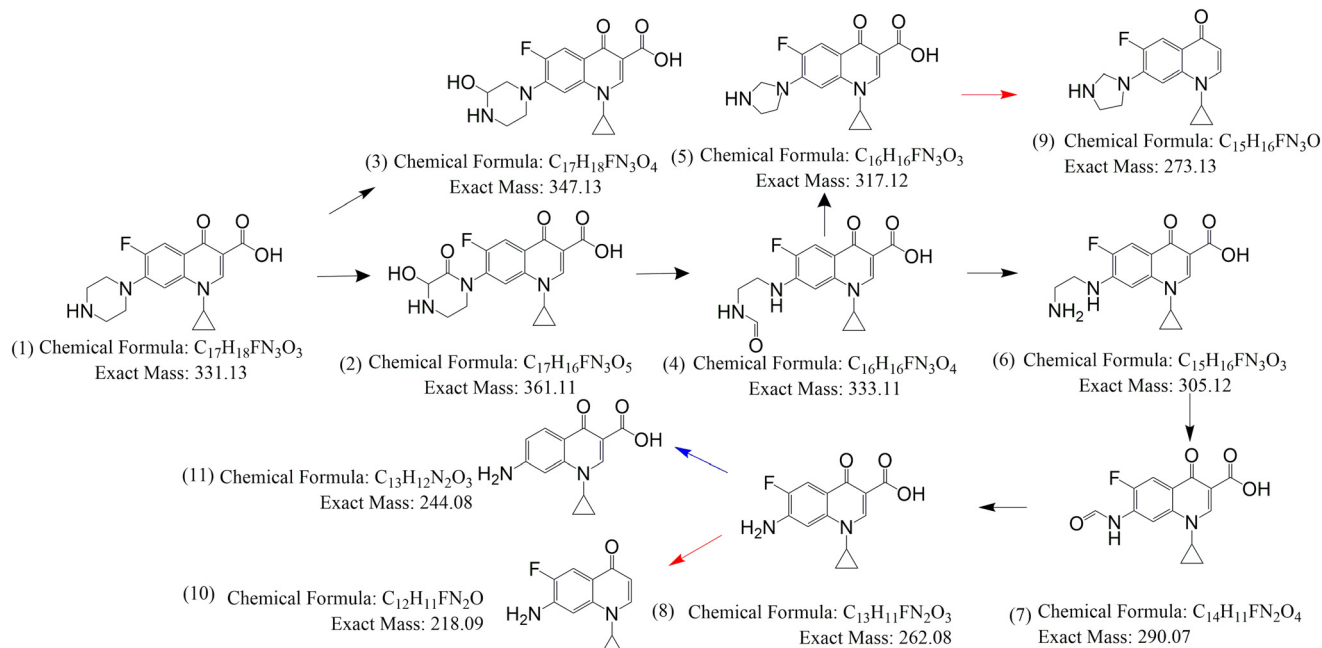
Scheme 1 Possible degradation mechanism of CIP by TP beads; TP = 1% TiO$_2$ with PVDF having 0.7% PVP.

polymeric membrane for water treatment in degrading the CIP, a widely detected antibiotic micropollutants with its antibacterial activity removed by an energy-efficient UVA LED light source.

4. Conclusion

The study presents the immobilization of TiO$_2$ with PVDF beads (TP) by the phase inversion method and photocatalytic degradation of CIP by TP under UVA LED irradiation. The SEM images reveal the TP bead with a sponge-like morphology and immobilization of TiO$_2$. The Ti–F coordination bond in TP revealed by XPS analysis was attributed to the effective immobilization of TiO$_2$ in the spongy beads. UVDRS and Mott-Schottky analysis showed no significant modification in the electronic properties of TiO$_2$ after immobilization with PVDF. The photocatalytic degradation of CIP obeyed pseudo first-

order kinetics with k_{obs} = 0.0761 min^{-1}. Excess PVP, a hydrophilic additive, hinders the photocatalytic activity due to the masking of TiO$_2$ nanoparticles. Highly acidic and basic pH conditions retarded the degradation efficiency. O$_2^{-•}$, h$^+$, HO$^•$, and ^{1}O$_2$ were identified as reactive species responsible for the degradation of CIP by TP according to the radical scavenging, photocurrent measurements and ESR. The efficient degradation of CIP was demonstrated in both tap water and surface groundwater. The easy recovery of TP beads from water was achieved by collecting the beads with a simple strainer. 30 cycles of photodegradation without the loss of TiO$_2$ from TP beads were demonstrated. The degradation of CIP molecule due to the oxidation of the piperazine ring and defluorination reactions were proposed for the generation of the degradation byproducts. Additionally, antibacterial assays showed the removal of the antibacterial activity after the TP photocatalytic degradation of CIP. Energy efficiency calculations revealed that TP photocatalysis is an energy-efficient water treatment method under UVA LED irradiation with easy recovery. The study highlights polymeric beads with TiO$_2$ obtained by the phase inversion technique as promising to enhance the usage of TiO$_2$ nanoparticles for water treatment.

Data availability statement

All the data is contained within the article.

Author contributions

Laxman G. Raikar: methodology, validation, formal analysis, investigation, writing – original draft, writing – review & editing, visualization, Atul Patel: methodology, investigation
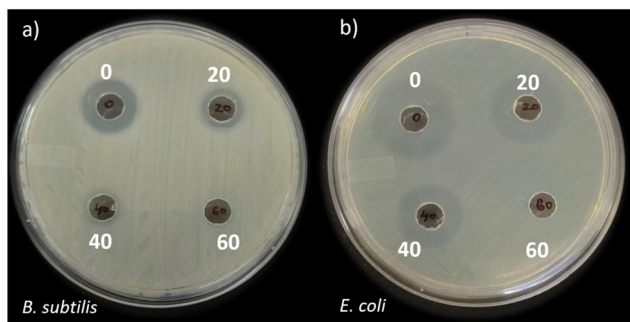

Fig. 12 Antibacterial activity of 1 ppm CIP (0) and 20, 40 and 60 min TP bead-treated CIP against (a) *B. subtilis* and (b) *E. coli*; TP = 1% TiO$_2$ with PVDF having 0.7% PVP.

3740 | *Environ. Sci.: Nano*, 2024, **11**, 3729–3743

This journal is © The Royal Society of Chemistry 2024

Conflicts of interest

There are no conflicts to declare.

Acknowledgements

References

1 Y. Tong, P. J. McNamara and B. K. Mayer, Adsorption of organic micropollutants onto biochar: a review of relevant kinetics, mechanisms and equilibrium, *Environ. Sci.: Water Res. Technol.*, 2019, **5**, 821–838.

2 J. F. Kerrigan, K. D. Sandberg, D. R. Engstrom, T. M. LaPara and W. A. Arnold, Small and large-scale distribution of four classes of antibiotics in sediment: association with metals and antibiotic resistance genes, *Environ. Sci.: Processes Impacts*, 2018, **20**, 1167–1179.

3 M. D. J. S. Chaves, J. Kulzer, P. D. R. Pujol De Lima, S. C. Barbosa and E. G. Primel, Updated knowledge, partitioning and ecological risk of pharmaceuticals and personal care products in global aquatic environments, *Environ. Sci.: Processes Impacts*, 2022, **24**, 1982–2008.

4 R. Andreozzi, Advanced oxidation processes (AOP) for water purification and recovery, *Catal. Today*, 1999, **53**, 51–59.

5 C. Byrne, G. Subramanian and S. C. Pillai, Recent advances in photocatalysis for environmental applications, *J. Environ. Chem. Eng.*, 2018, **6**, 3531–3555.

6 M. C. Dlamini, M. S. Maubane-Nkadimeng and J. A. Moma, The use of TiO2/clay heterostructures in the photocatalytic remediation of water containing organic pollutants: A review, *J. Environ. Chem. Eng.*, 2021, **9**, 106546.

7 A. Ajmal, I. Majeed, R. N. Malik, H. Idriss and M. A. Nadeem, Principles and mechanisms of photocatalytic dye degradation on TiO$_2$ based photocatalysts: a comparative overview, *RSC Adv.*, 2014, **4**, 37003–37026.

8 H. Ding and J. Hu, Degradation of ibuprofen by UVA-LED/TiO2/persulfate process: Kinetics, mechanism, water matrix effects, intermediates and energy consumption, *Chem. Eng. J.*, 2020, **397**, 125462.

9 D. E. Willis, E. C. Sheets, M. R. Worbington, M. Kamat, S. K. Glass, M. J. Caso, T. Ofoegbuna, L. M. Diaz, C. Osei-Appau, S. D. Snow and K. M. McPeak, Efficient Chemical-Free Degradation of Waterborne Micropollutants with an Immobilized Dual-Porous TiO$_2$ Photocatalyst, *ACS ES&T Eng.*, 2023, **3**, 1694–1705.

10 D. P. Utomo, T. D. Kusworo, A. C. Kumoro and M. H. D. Othman, Developing a versatile and resilient PVDF/CeO2@GO-COOH photocatalytic membrane for efficient treatment of antibiotic-contaminated wastewater, *J. Water Process Eng.*, 2023, **56**, 104353.

11 S. Xu, Y. Liu, Y. Yu, X. Zhang, J. Zhang and Y. Li, PAN/PVDF chelating membrane for simultaneous removal of heavy metal and organic pollutants from mimic industrial wastewater, *Sep. Purif. Technol.*, 2020, **235**, 116185.

12 H. S. Zakria, M. H. D. Othman, R. Kamaludin, S. H. S. A. Kadir, T. A. Kurniawan and A. Jilani, Immobilization techniques of a photocatalyst into and onto a polymer membrane for photocatalytic activity, *RSC Adv.*, 2021, **11**, 6985–7014.

13 A. Ashley, B. Thrope, M. R. Choudhury and A. H. Pinto, Emerging investigator series: photocatalytic membrane reactors: fundamentals and advances in preparation and application in wastewater treatment, *Environ. Sci.: Water Res. Technol.*, 2022, **8**, 22–46.

14 H. P. Ngang, B. S. Ooi, A. L. Ahmad and S. O. Lai, Preparation of PVDF–TiO2 mixed-matrix membrane and its evaluation on dye adsorption and UV-cleaning properties, *Chem. Eng. J.*, 2012, **197**, 359–367.

15 S. Wan, W. Zhao, D. Xiong, S. Li, Y. Ye and L. Du, Novel alginate immobilized TiO$_2$ reusable functional hydrogel beads with high photocatalytic removal of dye pollutions, *J. Polym. Eng.*, 2022, **42**, 978–985.

16 I. Dalponte Dallabona, Á. L. Mathias and R. M. M. Jorge, A new green floating photocatalyst with Brazilian bentonite into TiO2/alginate beads for dye removal, *Colloids Surf., A*, 2021, **627**, 127159.

17 S. Chkirida, N. Zari, R. Achour, H. Hassoune, A. Lachehab, A. E. K. Qaiss and R. Bouhfid, Highly synergic adsorption/photocatalytic efficiency of Alginate/Bentonite impregnated TiO2 beads for wastewater treatment, *J. Photochem. Photobiol., A*, 2021, **412**, 113215.

18 K. Wu, B. Li, X. Dong, P. Wu, K. Sun, S. Yang, J. Wu, J. Hou, Z. Liu and X. Guo, Flexible And Recyclable PPy-TiO$_2$@WO$_3$ Photocatalyst Supported By Cellulose Aerogel Beads, *ChemistrySelect*, 2020, **5**, 6527–6536.

19 D. Cani and P. P. Pescarmona, Macroscopic TiO2–SiO2 porous beads: Efficient photocatalysts with enhanced reusability for the degradation of pollutants, *J. Catal.*, 2014, **311**, 404–411.

20 S. K. Mehta, S. Kumar, S. Chaudhary and K. K. Bhasin, Nucleation and growth of surfactant-passivated CdS and HgS nanoparticles: Time-dependent absorption and luminescence profiles, *Nanoscale*, 2010, **2**, 145–152.

This journal is © The Royal Society of Chemistry 2024

Environ. Sci.: Nano, 2024, **11**, 3729–3743 | **3741**

21 N. M. Mokhtar, W. J. Lau, A. F. Ismail and B. C. Ng, Physicochemical study of polyvinylidene fluoride–Cloisite15A® composite membranes for membrane distillation application, *RSC Adv.*, 2014, **4**, 63367–63379.

22 L. G. Raikar, J. Gandhi, K. V. K. Gupta and H. Prakash, Degradation of Ampicillin with antibiotic activity removal using persulfate and submersible UVC LED: Kinetics, mechanism, electrical energy and cost analysis, *Chemosphere*, 2024, **349**, 140831.

23 S. Gupta, J. Gandhi, S. Kokate, L. G. Raikar, V. G. Kopuri and H. Prakash, Augmented photocatalytic degradation of Acetaminophen using hydrothermally treated g-C3N4 and persulfate under LED irradiation, *Heliyon*, 2023, **9**, e16450.

24 F. R. Cockerill, *Methods for dilution antimicrobial susceptibility tests for bacteria that grow aerobically: approved standard*, CLSI, Wayne, Pa, 9th edn, 2012.

25 T. M. H. Le, R. Wang and S. Sairiam, Self-protecting PVDF-PDA-TiO2 membranes towards highly efficient and prolonged dye wastewater treatment by photocatalytic membranes, *J. Membr. Sci.*, 2023, **683**, 121789.

26 M. O. Mavukkandy, M. R. Bilad, A. Giwa, S. W. Hasan and H. A. Arafat, Leaching of PVP from PVDF/PVP blend membranes: impacts on membrane structure and fouling in membrane bioreactors, *J. Mater. Sci.*, 2016, **51**, 4328–4341.

27 Z. Guo, X. Xu, Y. Xiang, S. Lu and S. P. Jiang, New anhydrous proton exchange membranes for high-temperature fuel cells based on PVDF–PVP blended polymers, *J. Mater. Chem. A*, 2015, **3**, 148–155.

28 O. T. Alaoui, Q. T. Nguyen, P. Schaetzel and C. Mbareck, Dye and bacteria photodegradations with anatase-loaded microporous poly(vinylidene fluoride) membranes, *Catal. Sci. Technol.*, 2011, **1**, 1412.

29 C.-L. Liang, Q. Xie, R.-Y. Bao, W. Yang, B.-H. Xie and M.-B. Yang, Induced formation of polar phases in poly(vinylidene fluoride) by cetyl trimethyl ammonium bromide, *J. Mater. Sci.*, 2014, **49**, 4171–4179.

30 Y. Zhang, G. Zhang, S. Liu, C. Zhang and X. Xu, "Naked" TiO2 capsulated in nanovoid microcapsule of poly(vinylidene fluoride) supporter with enhanced photocatalytic activity, *Chem. Eng. J.*, 2012, **204–206**, 217–224.

31 Z. Cui, N. T. Hassankiadeh, Y. Zhuang, E. Drioli and Y. M. Lee, Crystalline polymorphism in poly(vinylidenefluoride) membranes, *Prog. Polym. Sci.*, 2015, **51**, 94–126.

32 M. Wang, D. Fang, N. Wang, S. Jiang, J. Nie, Q. Yu and G. Ma, Preparation of PVDF/PVP core–shell nanofibers mats via homogeneous electrospinning, *Polymer*, 2014, **55**, 2188–2196.

33 N. D. Kulkarni and P. Kumari, Development of highly flexible PVDF-TiO2 nanocomposites for piezoelectric nanogenerator applications, *Mater. Res. Bull.*, 2023, **157**, 112039.

34 L. Ye, C. Yang, L. Tian, L. Zan and T. Peng, Tunable photocatalytic selectivity of fluoropolymer PVDF modified TiO2, *Appl. Surf. Sci.*, 2011, **257**, 8072–8077.

35 Z. Tian, Y. Song, J. Zhang, S. Qin, Y. Yang, J. Li and Z. Cui, In situ growth of TiO2 and its immobilization on PVDF films

for the adsorption and photocatalytic degradation of dye, *Int. J. Hydrogen Energy*, 2024, **51**, 837–847.

36 S. N. S. Nasir, N. A. Mohamed, M. A. Tukimon, M. F. M. Noh, N. A. Arzaee and M. A. M. Teridi, Direct extrapolation techniques on the energy band diagram of BiVO4 thin films, *Phys. B*, 2021, **604**, 412719.

37 N. Agrawal, R. S. Ray, M. Farooq, A. B. Pant and R. K. Hans, Photosensitizing Potential of Ciprofloxacin at Ambient Level of UV Radiation: Photochemistry and Photobiology, 2007, 83, *Photochem. Photobiol.*, 2007, **83**, 1226–1236.

38 X. Zheng, Y. Liu, X. Liu, Q. Li and Y. Zheng, A novel PVDF-TiO2@g-C3N4 composite electrospun fiber for efficient photocatalytic degradation of tetracycline under visible light irradiation, *Ecotoxicol. Environ. Saf.*, 2021, **210**, 111866.

39 A. Balakrishnan, M. Chinthala and R. K. Polagani, 3D kaolinite/g-C3N4-alginate beads as an affordable and sustainable photocatalyst for wastewater remediation, *Carbohydr. Polym.*, 2024, **323**, 121420.

40 J. Ma, Y. Tang, G. Lu, Y. Wang, W. Niu, D. Fu, K. Zhang, D. W. Bahnemann and J. H. Pan, Incorporating Mesoporous Anatase TiO2 Spheres to Conductive Carbon Black Filled PVDF Membrane for Self-Cleaning Photo(electro)catalytic Filtration, *J. Phys. Chem. C*, 2023, **127**, 7998–8005.

41 M. Manjunatha and H. Mahalingam, Upcycling of waste EPS beads to immobilized codoped TiO2 photocatalysts for ciprofloxacin degradation and E. coli disinfection under sunlight, *Sci. Rep.*, 2023, **13**, 14631.

42 E. Erusappan, S. Thiripuranthagan, R. Radhakrishnan, M. Durai, S. Kumaravel, T. Vembuli and N. J. Kaleekkal, Fabrication of mesoporous TiO2/PVDF photocatalytic membranes for efficient photocatalytic degradation of synthetic dyes, *J. Environ. Chem. Eng.*, 2021, **9**, 105776.

43 C. Chen, S. Wang, F. Han, X. Zhou and B. Li, Synergy of rapid adsorption and photo-Fenton-like degradation in CoFe-MOF/TiO2/PVDF composite membrane for efficient removal of antibiotics from water, *Sep. Purif. Technol.*, 2024, **333**, 125942.

44 A. R. Lado Ribeiro, N. F. F. Moreira, G. Li Puma and A. M. T. Silva, Impact of water matrix on the removal of micropollutants by advanced oxidation technologies, *Chem. Eng. J.*, 2019, **363**, 155–173.

45 Y.-J. Lee, Y. Jae Jeong, I. Sun Cho, C.-G. Lee, S.-J. Park and P. J. J. Alvarez, The inhibitory mechanism of humic acids on photocatalytic generation of reactive oxygen species by TiO2 depends on the crystalline phase, *Chem. Eng. J.*, 2023, **476**, 146785.

46 A. Bianco, M. I. Polo-López, P. Fernández-Ibáñez, M. Brigante and G. Mailhot, Disinfection of water inoculated with Enterococcus faecalis using solar/Fe(III)EDDS-H2O2 or S2O82− process, *Water Res.*, 2017, **118**, 249–260.

47 C.-R. Zhong, T.-W. Lee, J.-A. Li, Y.-H. Lai, T.-J. Ha and C. Chen, Origin of the enhanced photocatalytic activity of graphitic carbon nitride nanocomposites and the effects of water constituents, *Carbon*, 2020, **167**, 852–862.

48 J. Gandhi and H. Prakash, Photo-disinfection processes for bacterial inactivation and underlying principles for water

3742 | *Environ. Sci.: Nano*, 2024, **11**, 3729–3743

This journal is © The Royal Society of Chemistry 2024

constituents' impact: A review, *Chem. Eng. J. Adv.*, 2023, **14**, 100482.

49 N. Jallouli, L. M. Pastrana-Martínez, A. R. Ribeiro, N. F. F. Moreira, J. L. Faria, O. Hentati, A. M. T. Silva and M. Ksibi, Heterogeneous photocatalytic degradation of ibuprofen in ultrapure water, municipal and pharmaceutical industry wastewaters using a TiO2/UV-LED system, *Chem. Eng. J.*, 2018, **334**, 976–984.

50 T. An, H. Yang, G. Li, W. Song, W. J. Cooper and X. Nie, Kinetics and mechanism of advanced oxidation processes (AOPs) in degradation of ciprofloxacin in water, *Appl. Catal., B*, 2010, **94**, 288–294.

51 T. Ahamad, Mu. Naushad and S. M. Alshehri, Analysis of degradation pathways and intermediates products for ciprofloxacin using a highly porous photocatalyst, *Chem. Eng. J.*, 2021, **417**, 127969.

52 X. Zheng, S. Xu, Y. Wang, X. Sun, Y. Gao and B. Gao, Enhanced degradation of ciprofloxacin by graphitized mesoporous carbon (GMC)-TiO2 nanocomposite: Strong synergy of adsorption-photocatalysis and antibiotics degradation mechanism, *J. Colloid Interface Sci.*, 2018, **527**, 202–213.

53 D. Wu, J. Li, J. Guan, C. Liu, X. Zhao, Z. Zhu, C. Ma, P. Huo, C. Li and Y. Yan, Improved photoelectric performance via fabricated heterojunction g-C3N4/TiO2/HNTs loaded photocatalysts for photodegradation of ciprofloxacin, *J. Ind. Eng. Chem.*, 2018, **64**, 206–218.

54 J. Feng, L. Wang, X. Ran, B. Xiao, L. Lei, J. Zhu, R. Li, X. Xi and G. Feng, Adsorption and photocatalytic synergistic removal of ciprofloxacin on mesoporous ErFeO3/g-C3N4 heterojunction, *Environ. Technol. Innovation*, 2022, **28**, 102785.

55 S. Kokate, S. Gupta, V. G. Kopuri and H. Prakash, Energy efficient photocatalytic activation of peroxymonosulfate by g-C3N4 under 400 nm LED irradiation for degradation of Acid Orange 7, *Chemosphere*, 2022, **287**, 132099.

This journal is © The Royal Society of Chemistry 2024

Environ. Sci.: Nano, 2024, **11**, 3729–3743 | **3743**